

A constitutive relation describing the shear-banding transition

Jan K. G. Dhont

*Van 't Hoff Laboratory for Physical and Colloid Chemistry, Debye Institute, Utrecht University, Padualaan 8,
3584 CH Utrecht, The Netherlands*

(Received 8 February 1999)

An additional contribution to the standard expression for the shear stress must be considered in order to describe shear banding. A possible extension of the standard constitutive relation is proposed. Its physical, purely hydrodynamic origin is discussed. The corresponding Navier-Stokes equation is analyzed for the two-plate geometry, where flow gradients are assumed to exist only in the direction perpendicular to the two plates. The linearized Navier-Stokes equation is shown to be very similar to the Cahn-Hilliard equation for spinodal decomposition, with a similar term that stabilizes rapid spatial variations. Only slowly varying flow gradients are unstable. Just as in the initial stage of spinodal decomposition there is a most rapidly growing wavelength in the initial stage of the shear-banding transition, leading to a predictable number of shear bands. A modified Maxwell equal area construction is derived, which dictates the stress and the shear rates in the bands under controlled shear conditions, and which shows that under controlled stress conditions no true shear bands can coexist. The kinetics of the shear-banding transition is studied numerically. For the two-plate geometry it is found that there exist multiple stationary states under controlled shear conditions, depending on the initial state of the flow profile. Shear banding occurs not only when the system is initially unstable, but can also be induced outside the unstable region when the amplitude of the initial perturbation is large enough. The shear-banding transition can thus proceed via “spinodal demixing” (from an unstable initial state) or via “condensation.” Under controlled stress conditions no stationary state is found. Here, coupling with flow gradients extending in other directions, not perpendicular to the two plates, should probably be taken into account. [S1063-651X(99)18310-7]

PACS number(s): 83.20.Bg, 47.15.Fe

I. INTRODUCTION

In many fluids containing mesoscopic entities, a mechanical instability (or metastability) can be induced by applying shear flow, where the system ultimately “demixes” in regions of high and low shear rates. These “bands” of constant high and low shear rates are connected by “interfaces,” where sharp spatial changes of the local shear rate occur. This so-called shear-banding instability occurs when the stress versus the shear rate of a homogeneously sheared system, prior to the transition, exhibits a van der Waals-like behavior, where there is a range of shear rates where the stress decreases with increasing shear rate. This transition has a *mechanical, hydrodynamic origin*.

Thermodynamically driven transitions, which also occur in the absence of shear flow, will be affected by shearing motion. Both the kinetics of phase separation and the location of phase boundaries are changed by applying shear flow. The thermodynamic forces which drive the transition will generally be affected by shearing motion in a way that is far from understood. If one is willing to accept the concept of local thermodynamic equilibrium in systems under shear flow, these forces can be formulated within the framework of irreversible thermodynamics [1–3]. The forces that drive these types of phase transitions of systems in shearing motion have a *thermodynamic origin*.

It is not always possible to strictly distinguish between mechanical and thermodynamic instabilities. First of all these forces can be at work simultaneously, where coupling between the two may be essential for an instability to occur. Moreover, shear forces may induce entirely new microstruc-

tural order (for example, in surfactant systems), which may lead to phase transitions that are in turn driven by forces of a thermodynamic nature. Here, forces of a thermodynamic nature are put to work to drive a transition between states that can exist only under the influence of shear forces.

The aim of this paper is to introduce a physically plausible extension of the standard constitutive relation, and to study the demixing kinetics from an initially perturbed state of constant shear rate to the stationary shear-banded state. The proposed constitutive relation should be employed in describing the more complicated situation where shear forces and thermodynamic forces are intertwined.

Shear banding has been unambiguously observed, or there are strong indications for its occurrence, for wormlike micelles [4–7] (which sometimes show an isotropic-nematic phase transition in the absence of shear flow) in other surfactant systems [8,9] (which exhibit a reentrant transition of a lyotropic lamellar phase to a phase of multilayered vesicles) and in polycrystalline colloids [10–12]. In some cases the shear-banding transition seems to occur in the vicinity of a thermodynamic phase boundary. It may be that a van der Waals-like behavior of the stress is enhanced by pretransitional thermodynamic phenomena.

The shear-banding instability has been analyzed for the case of flow through a cylindrical pipe by McLeish *et al.* [13,14], assuming that a single, infinitely sharp interface exists. The Navier-Stokes equation is then solved, imposing boundary conditions on the interface and using the standard constitutive relation for the stress with an expression for the viscosity as derived for entangled polymer systems [15–17]. Recently, Spenley *et al.* [18] and Porte *et al.* [19] formulated

nonstandard constitutive relations for the stress, in order to predict shear banding without having to assume the existence of a single, infinitely sharp interface. Porte *et al.* use quasi-thermodynamic arguments to construct a constitutive equation, while Spenley *et al.* introduce a simple constitutive relation that exhibits both viscoelastic behavior and nonlinear response.

In the present paper a natural extension of the standard constitutive relation is proposed that introduces a higher order spatial derivative of the shear rate. Such a gradient contribution to the stress is essential to describe the interfaces. It is argued that this higher order derivative is of a purely hydrodynamic nature. The shear-banding transition considered in the present paper is studied without consideration of non-local contributions from the equilibrium free energy that couples to inhomogeneities in microstructure nor the intervening effects of forces that may drive a phase transition. Including such contributions in order to describe shear banding gives rise to gradient contributions to the stress [2,3], which, however, do not depend on the local shear rate, contrary to the purely hydrodynamic contribution. There is a very recent preprint database [20] in which ideas similar to those in the present paper are formulated.

This paper is organized as follows. In Sec. II it is argued that higher order derivatives contribute to the stress. Arguments are based on considerations of the effect of shear flow on microstructural order. A phenomenological coefficient is introduced that will be referred to as “the shear-curvature viscosity.” It is argued that the shear-curvature viscosity shear thins to 0 in the same shear rate range where the shear viscosity shear thins to its high shear rate plateau value. In addition, the corresponding Navier-Stokes equation and the boundary conditions under controlled shear and stress conditions are formulated for the two-plate geometry. A modified Maxwell equal area construction is derived in Sec. III. This Maxwell construction predicts the shear rates in the high and low shear rate regions of the shear-banded structure and the stress in the stationary state. It also shows that no true shear-banded structure (where the shear rate is constant within regions of finite extent) can exist under controlled stress conditions. A linear stability analysis is given in Sec. IV, both under controlled shear and controlled stress conditions. It is shown that in the initial stage there is a most rapidly growing wavelength, quite analogous to the Cahn-Hilliard scenario for spinodal decomposition. It is predicted that the linear instability disappears when the system size is small enough, which would allow the measurement of the entire van der Waals looplike behavior of the stress, using for example a Couette geometry with a very small gap width. In Sec. V it is argued that there is no unique stationary shear-banded flow for the two-plate geometry. This is confirmed in Sec. VI, where the full nonlinear, time dependent Navier-Stokes equation is solved numerically. The most rapidly growing wavelength dominates the flow pattern in the early stages of the shear-banding transition. This leads to a generic number of interfaces in the final stationary state. It turns out that under controlled shear conditions there exist “spinodal and binodal shear rates”: in certain shear rate intervals the transition to the shear-banded state may occur because the initial flow is linearly unstable (“spinodal decomposition”), or occurs only due to perturbations with some minimum, finite

amplitude (“condensation”). Under controlled stress conditions no convergence to a stationary state is found within the one-dimensional treatment of the two-plate geometry. The possible reasons for this are discussed. Section VII is a summary and discussion.

II. THE CONSTITUTIVE RELATION AND THE CORRESPONDING NAVIER-STOKES EQUATION

Consider a laminar flow between two flat plates, where the fluid velocity \mathbf{u} is along the x direction parallel to the two plates and depends only on the distance y from the lower, stationary plate. The Navier-Stokes equation for such a flow reads

$$\rho \frac{\partial u(y,t)}{\partial t} = \frac{\partial \Sigma(y,t)}{\partial y}, \quad (1)$$

with ρ the mass density and Σ the stress. Diffusive mass transport will not be considered, and the mass density ρ will be taken constant in the sequel. Diffusive mass transport may under certain circumstances be important [21,22]. When one is away from the thermodynamic spinodal region, where the effective diffusion coefficient is negative, and as long as the “feedback instability” does not occur [21,22], diffusive mass transport probably does not affect the essential features of the shear-banding transition. It is also assumed that the shear-banding transition is sufficiently slow to neglect the elastic contribution to the stress response. Depending on how fast the shear-banding transition occurs in comparison to typical microstructural relaxation times, one could extend the constitutive relation that is proposed in the present paper to include elastic response (for example, with a simple Maxwell relaxation model). Including elastic stresses would interfere with the clarity of arguments related to the essential features of shear banding, so that an account of elasticity is deferred to a future work.

The standard constitutive relation for the stress Σ , without elastic contributions, reads

$$\Sigma(y,t) = \eta(\dot{\gamma}(y,t)) \dot{\gamma}(y,t), \quad (2)$$

where $\dot{\gamma}(y,t) = \partial u(y,t)/\partial y$ is the local shear rate and η is the shear viscosity. It follows from Eq. (1) that in a stationary state we must have a constant stress throughout the system,

$$\Sigma(y,t) = \text{const} \quad (\text{for stationary states}), \quad (3)$$

which expresses mechanical stability. As is well known, this equation cannot be satisfied in a shear-banded state, where $\eta \dot{\gamma}$ exhibits a van der Waals-like behavior: in the low and high shear rate regions this equation can be satisfied, but in passing through an interface, the stress varies according to the van der Waals loop and is therefore not a constant. The standard constitutive relation (2) for the stress is therefore not sufficient to describe shear banding.

Let us first ask for the physical meaning of the standard constitutive equation (2). This relation simply assumes that the friction force between two adjacent, sliding layers of fluid [as depicted in Fig. 1(a)] is proportional to their relative velocity, that is, to the shear rate. The friction coefficient of two sliding layers, which is the proportionality constant be-

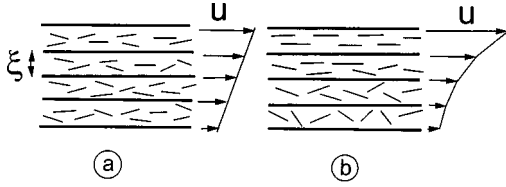


FIG. 1. (a) Sliding layers in a system of rodlike particles, where the shear rate is constant over length scales of the order of the length of the rods. (b) Sliding layers in the same system, where the shear rate changes appreciably over such length scales.

tween the friction force (stress) and the relative velocity (shear rate) of the layers, is the shear viscosity. The viscosity itself is shear rate dependent, because the friction coefficient of two adjacent layers depends on the microstructural order in those layers. For example, in the case of a suspension of rigid rods, the friction coefficient (shear viscosity) will be different for an almost isotropic arrangement of the rods as compared to a highly aligned microstructural order.

Now suppose that the shear rate changes on a length scale of the order of the range ξ of interactions between the mesoscopic entities in the system. For example, for a stable system of stiff, rodlike particles the range of interactions is of the order of the length of the rods. The microstructural order is then significantly different in adjacent sliding layers of fluid, as depicted in Fig. 1(b). Although the average shear rate over the two middle layers in Fig. 1(b) is the same as in Fig. 1(a), the friction force between these two layers will be different from those in Fig. 1(a), simply because the microstructural order of the middle two sliding layers in Fig. 1(b) is different. The effect of such differences in shear induced microstructural order in adjacent sliding layers on the friction force is clearly related to spatial derivatives of the shear rate. The constitutive relation now contains contributions from spatial derivatives of the shear rate.

The formal construction of the standard constitutive relation, which can be found in any textbook on hydrodynamics, is based on the assumption that only first-order spatial derivatives of the fluid flow velocity contribute to the stress. The leading order term in a formal expansion with respect to gradients in the flow velocity leads to the standard constitutive relation (2). As explained above, in the case of rapid spatial variation of the fluid flow velocity, the next higher order term in this formal expansion will be important as well.

There are three candidates for the next higher order contribution to the stress in a formal expansion with respect to gradients in the velocity: $\sim \partial \dot{\gamma}(y,t)/\partial y$, $\sim [\partial \dot{\gamma}(y,t)/\partial y]^2$ and $\sim \partial^2 \dot{\gamma}(y,t)/\partial y^2$. The stress changes sign when the shear rate changes sign and is invariant under coordinate inversion (where y is replaced by $-y$). The first of the above candidates is not invariant under coordinate inversion (note that $\dot{\gamma}$ is invariant), while the second does not change sign when the $\dot{\gamma}$ is changed in sign. The first two above mentioned derivatives do not comply with the symmetry properties of the stress and are therefore absent in a formal expansion of the stress with respect to spatial gradients in the velocity. The third candidate, however, complies with both symmetry requirements, and is therefore the relevant additional term.

In molecular systems this higher order term is never considered, because the range of interactions in these systems is very small. In colloidal and macromolecular systems, how-

ever, particles are much bigger, and relatively small shear rate gradients are already sufficient to contribute to the stress.

We thus arrive at the following expression for the stress:

$$\Sigma(y,t) = \eta(\dot{\gamma}(y,t))\dot{\gamma}(y,t) - \kappa(\dot{\gamma}(y,t))\frac{\partial^2 \dot{\gamma}(y,t)}{\partial y^2}. \quad (4)$$

The proportionality constant κ is referred to here as “the shear-curvature viscosity.” The same expression for the stress has been proposed very recently in a preprint database [20].

The shear-curvature viscosity κ is shear rate dependent because a difference of the shear rate in two adjacent layers induces a difference in their microstructure in a way that is dependent on the average local shear rate. In the case where the local shear rate is very large, so that the microstructure is saturated by the shear flow in both layers, an additional change of the shear rate in the two layers does not affect their microstructure, and hence does not change the stress. For dispersions of rodlike particles, for example, the alignment will be almost perfect for high local shear rates, so that the effect of a shear rate gradient hardly affects the alignment in the two layers. The shear-curvature contribution to the stress must therefore vanish for shear rates so large that the microstructure is saturated by the shear forces. This is precisely the shear rate where the shear viscosity reaches its high shear plateau value. The shear-curvature viscosity therefore shears to zero,

$$\lim_{\dot{\gamma} \rightarrow \infty} \kappa(\dot{\gamma}) = 0. \quad (5)$$

Both η and κ have well defined low and high shear rate limits. Low shear rate limiting values relate to friction between sliding layers with a linearly perturbed, almost isotropic microstructure, while the high shear rate limiting values relate to sliding layers with a microstructure that is saturated by the local shear rate.

Equation (3) for a stationary state now reads

$$\eta(\dot{\gamma}(y))\dot{\gamma}(y) - \kappa(\dot{\gamma}(y))\frac{d^2 \dot{\gamma}(y)}{dy^2} = \Sigma_{stat}, \quad (6)$$

where the time dependence is omitted and Σ_{stat} is the stress in the stationary state, which is independent of y and t . The question now arises whether this expression can be satisfied in a stationary shear-banded state. Consider a low and high shear rate region connected by an interface, as depicted in Fig. 2(a). Going through the interface the contribution $\eta(\dot{\gamma})\dot{\gamma}$ to the stress traces its van der Waals loop, as depicted in Fig. 2(b) [this figure is constructed from Fig. 2(a) with the use of the expression (33) for σ that is used for numerical computations; the shear rate dependence of σ is plotted in Fig. 3(a)]. The third order derivative $\partial^3 u(y)/\partial y^3$ is depicted in Fig. 2(c). This derivative has the same symmetry as $\eta(\dot{\gamma})\dot{\gamma}$, and is thus indeed the proper candidate to ensure a constant stress throughout the suspension in the stationary shear-banded state. Note that the contribution to the total stress is obtained by multiplying the third-order derivative with $\kappa(\dot{\gamma})$, which increases with increasing y in this example, thus weighting the maximum more strongly than the minimum in Fig. 2(c).

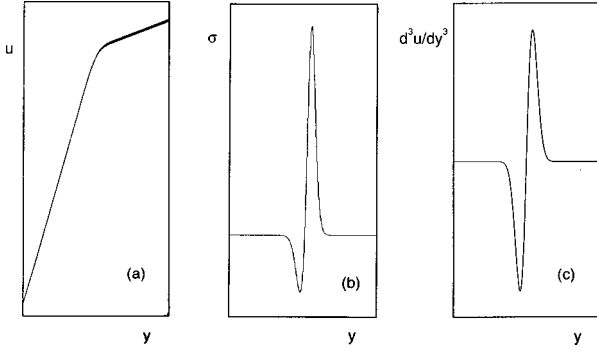


FIG. 2. (a) A low and high shear rate region, connected by an interface. (b) The variation of the stress $\eta(\dot{\gamma})\dot{\gamma}$ for the fluid flow depicted in (a). (c) The variation of $\partial^3 u(y)/\partial y^3$ for the fluid flow depicted in (a).

To assure a constant stress in the stationary state, the variations in the standard stress [see Fig. 2(b)] must cancel against the same variations resulting from the curvature induced stress [see Fig. 2(c)]. The curve in Fig. 2(c) must be *subtracted* from the standard stress to achieve this cancellation. We therefore added a minus sign to the shear-curvature stress contribution in Eq. (4): this ensures that the shear-curvature viscosity is positive.

Substitution of the extended constitutive relation (4) for the stress into Eq. (1) yields the following Navier-Stokes equation for the two-plate geometry:

$$\rho \frac{\partial u(y,t)}{\partial t} = \frac{d\sigma(\dot{\gamma}(y,t))}{d\dot{\gamma}(y,t)} \frac{\partial \dot{\gamma}(y,t)}{\partial y} - \kappa(\dot{\gamma}(y,t)) \frac{\partial^3 \dot{\gamma}(y,t)}{\partial y^3} - \frac{d\kappa(\dot{\gamma}(y,t))}{d\dot{\gamma}(y,t)} \frac{\partial \dot{\gamma}(y,t)}{\partial y} \frac{\partial^2 \dot{\gamma}(y,t)}{\partial y^2}, \quad (7)$$

where $\sigma(\dot{\gamma}) = \eta(\dot{\gamma})\dot{\gamma}$ is the stress in the direction of the flow without the shear-curvature contribution. The boundary conditions depend on whether a given overall shear rate $\dot{\gamma}_0$ is imposed or a given stress σ_0 is imposed. These correspond to experiments ‘‘under controlled shear’’ and ‘‘controlled stress,’’ respectively. The boundary conditions for the two-plate geometry for these two cases read

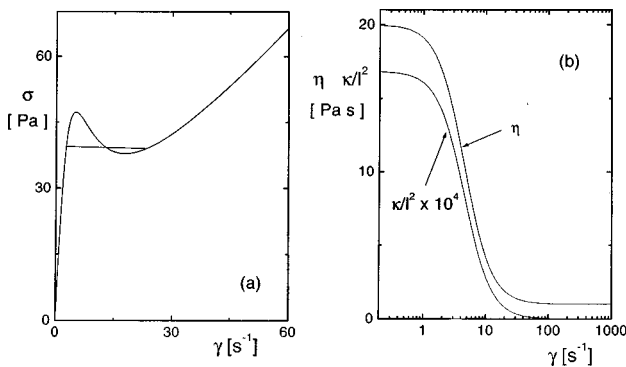


FIG. 3. (a) The stress $\sigma = \eta\dot{\gamma}$ versus the shear rate, according to Eq. (33), where the horizontal line corresponds to the modified Maxwell equal area construction (10). (b) The shear rate dependence of the shear viscosity η and the shear-curvature viscosity κ according to Eqs. (33) and (34), respectively.

$$u(y=l,t) = \dot{\gamma}_0 l \quad (\text{controlled shear}), \quad (8)$$

$$\Sigma(y=l,t) = \sigma_0 \quad (\text{controlled stress}), \quad (9)$$

while in both cases, $u(y=0,t) = 0$. Here, l is the gap width. The upper plate is given a prescribed, fixed velocity under controlled shear conditions, while under controlled stress conditions a constant force is exerted on the upper plate. In both cases the velocity of the fluid at the lower plate remains zero.

The above equations relate to the two-plate geometry. Additional terms are found in Eq. (7) in case of a Couette geometry, related to the curvature of the cylinders. The role of these additional terms will not be analyzed in the present paper.

III. MAXWELL EQUAL AREA CONSTRUCTION

Consider a low and high shear rate phase connected through an interface, as depicted in Fig. 2(a). When this is a stationary state, integration of Eq. (6) from $\dot{\gamma}_-$ to $\dot{\gamma}_+$ (the shear rates of the low and high shear rate regions, respectively) yields (see also Ref. [20])

$$\int_{\dot{\gamma}_-}^{\dot{\gamma}_+} d\dot{\gamma} [\sigma(\dot{\gamma}) - \Sigma_{stat}] / \kappa(\dot{\gamma}) = 0, \quad (10)$$

where (with y_- and y_+ the location of the low and high shear phases, respectively)

$$\int_{\dot{\gamma}_-}^{\dot{\gamma}_+} d\dot{\gamma} \frac{\partial^2 \dot{\gamma}}{\partial y^2} = \frac{1}{2} \int_{y_-}^{y_+} dy \frac{\partial}{\partial y} \left(\frac{\partial \dot{\gamma}}{\partial y} \right)^2 = 0 \quad (11)$$

is used. The last equality follows from the fact that in the low and high shear rate phases $\dot{\gamma}$ is constant, independent of y . This is a fundamental result for selection of $\dot{\gamma}_\pm$ and the total stress (in case of controlled shear conditions).

When κ is taken to be independent of the shear rate, Eq. (10) reduces to

$$\int_{\dot{\gamma}_-}^{\dot{\gamma}_+} d\dot{\gamma} \sigma(\dot{\gamma}) = \Sigma_{stat} (\dot{\gamma}_+ - \dot{\gamma}_-). \quad (12)$$

The stress Σ_{stat} is equal to $\sigma(\dot{\gamma}_-) = \sigma(\dot{\gamma}_+)$, since in the low and high shear rate regions the shear-curvature contribution to the stress vanishes. Therefore, Eq. (12) implies stress selection by a Maxwell equal area construction in the stress σ versus shear rate plane.

As discussed before, there are compelling reasons for the shear-thinning behavior of κ in the same shear rate range where η shear thins. Therefore the assumption of a constant value for κ , independent of the shear rate, is wrong, so that in reality the equal area construction does not apply. Stress selection under controlled shear conditions is described by Eq. (10), not by the equal area construction (12). The result in Eq. (10) will be referred to hereafter as ‘‘the modified Maxwell equal area construction.’’

Notice that under controlled stress conditions the total stress Σ_{stat} has a prescribed value. This implies that under controlled stress conditions the system either attains a stationary state with a constant shear rate $\dot{\gamma}$ such that $\sigma(\dot{\gamma})$

$=\Sigma_{stat}$, or that there exists a ‘‘blurred’’ shear-banded structure, where there are no regions in which the shear rate is a true constant.

IV. LINEAR STABILITY ANALYSIS

Let $\delta u(y,t)$ denote the small deviation from a flow profile with a spatially constant shear rate $\dot{\gamma}_0$ and the corresponding stress $\sigma_0 = \sigma(\dot{\gamma}_0)$. Linearization of Eq. (7) with respect to the small perturbation gives

$$\rho \frac{\partial \delta u(y,t)}{\partial t} = \frac{d\sigma(\dot{\gamma}_0)}{d\dot{\gamma}_0} \frac{\partial^2 \delta u(y,t)}{\partial y^2} - \kappa(\dot{\gamma}_0) \frac{\partial^4 \delta u(y,t)}{\partial y^4}. \quad (13)$$

The constraints under which this equation of motion must be solved are different for controlled shear and stress conditions. The limiting stability points of Eq. (13) will be established below, both under controlled shear and stress conditions.

A. Controlled shear conditions

The solution of the equation of motion (13) can be written as a Fourier series on the interval $[0,l]$, with l the distance between the two plates. The constraint that the velocity at the lower plate is equal to zero, that is, $\delta u(y=0,t)=0$, can be taken into account by extending the solution antisymmetrically to the interval $[-l,l]$. Without loss of generality, the solution can thus be written as a sine-series expansion on the interval $[-l,l]$,

$$\delta u(y,t) = \sum_{n=1}^{\infty} \alpha_n(t) \sin\{k_n y\}, \quad (14)$$

where the wave numbers k_n are equal to

$$k_n = \frac{\pi n}{l}, \quad n = 1, 2, 3, \dots \quad (15)$$

The solution (14) also satisfies the constraint $\delta u(y=l,t)=0$ that is imposed under controlled shear conditions. Substitution into Eq. (13) thus immediately leads to

$$\delta u(y,t) = \sum_{n=1}^{\infty} \alpha_n \sin\{k_n y\} \times \exp\left(-\left[\frac{d\sigma(\dot{\gamma}_0)}{d\dot{\gamma}_0} + \kappa(\dot{\gamma}_0)k_n^2\right] \frac{k_n^2 t}{\rho}\right). \quad (16)$$

The coefficients $\alpha_n \equiv \alpha_n(t=0)$ determine the initial perturbation $\delta u(y,t=0)$.

It is clear from Eq. (16) that a velocity profile with a constant shear rate is unstable when $d\sigma(\dot{\gamma}_0)/d\dot{\gamma}_0 < -\kappa(\dot{\gamma}_0)\pi^2/l^2 < 0$. In that case all Fourier modes with a wave number less than the critical wave number k_{crit} ,

$$k_{crit} = \sqrt{-\frac{d\sigma(\dot{\gamma}_0)/d\dot{\gamma}_0}{\kappa(\dot{\gamma}_0)}}, \quad (17)$$

grow exponentially in time (remember that $\kappa > 0$, as discussed in sec. II). Fourier modes with a wave number larger than k_{crit} are stable and decrease exponentially fast in amplitude.

Note that σ is equal to the total stress only when the system is homogeneously sheared, that is, when the shear rate is a constant throughout the gap. Hence, the negative slope of σ versus $\dot{\gamma}$ refers to the measured stress in a homogeneously sheared system, before the shear-banding transition occurred. In experiments the actually measured stress is that of a shear-banded state, which is different from the stress σ .

The interpretation of the part of the curve of σ versus $\dot{\gamma}$ where $d\sigma(\dot{\gamma})/d\dot{\gamma} < -\kappa(\dot{\gamma})\pi^2/l^2$ is as follows. A flow with constant shear rate $\dot{\gamma}$ will remain stable, even if $d\sigma(\dot{\gamma})/d\dot{\gamma} < -\kappa(\dot{\gamma})\pi^2/l^2$, when the gap width l is smaller than the critical wavelength $\lambda_{crit} = 2\pi/k_{crit}$. In that case all the unstable wavelengths are larger than the gap width, and no shear banding occurs. For such small gap widths the stress σ is well defined for all shear rates: that part of the van der Waals loop where $d\sigma(\dot{\gamma})/d\dot{\gamma} < -\kappa(\dot{\gamma})\pi^2/l^2$ is the stress that one would measure by standard means, with a rheometer where the gap width is so small that the unstable wavelengths $\lambda_n = 2\pi/k_n$ ‘‘do not fit into the gap.’’

The most rapidly growing wave number is the wave number closest to the wave number k_{max} ,

$$k_{max} = \sqrt{-\frac{d\sigma(\dot{\gamma}_0)/d\dot{\gamma}_0}{2\kappa(\dot{\gamma}_0)}} = \frac{k_{crit}}{\sqrt{2}}. \quad (18)$$

The fact that there is a most rapidly growing wavelength renders the state of the system in the initial stage of the shear-banding transition relatively insensitive to the initial state, provided that the initial amplitude of the perturbation is small. The number of bands in the initial stage of demixing is then equal to l/λ_{max} , with $\lambda_{max} = 2\pi/k_{max}$. The positions of the bands, however, depend sensitively on the structure of the initial perturbation.

There is a strong analogy between the above initial demixing scenario for shear banding and spinodal demixing kinetics. The Cahn-Hilliard equation of motion for the density of a thermodynamically unstable system [23,24] has the same structure as the linearized Navier-Stokes equation (13). The last term in the Navier-Stokes equation (13) corresponds to the ‘‘square-gradient contribution’’ to the free energy in the Cahn-Hilliard equation. This term stabilizes concentration variations of small wavelength, corresponding to large density gradients. Such rapid spatial concentration variations give rise to a relatively large increase in the free energy and are therefore stable as compared to long wavelength density variations. Similarly, the last term in the Navier-Stokes equation (13) stabilizes rapid spatial variations of the flow since these contribute relatively much to the stress.

B. Controlled stress conditions

Under controlled stress conditions the most general form of $\delta u(y,t)$, which satisfies the constraint $\delta u(y=0,t)=0$ reads

$$\delta u(y,t) = \delta \dot{\gamma}(t)y + \sum_{n=1}^{\infty} \alpha_n(t) \sin\{k_n y\}, \quad (19)$$

where the wave numbers are given in Eq. (15). The difference with the form (14), appropriate under controlled shear conditions, is the term $\delta \dot{\gamma}(t)y$, where $\delta \dot{\gamma}(t) = \dot{\gamma}(t) - \dot{\gamma}_0$ is the difference between the actual overall shear rate and the initial shear rate, the difference of which is generally nonzero under controlled stress conditions. Differentiation of Eq. (19) with respect to y yields

$$\delta \dot{\gamma}(y,t) = \sum_{n=0}^{\infty} \beta_n(t) \cos\{k_n y\}, \quad (20)$$

with $\beta_0(t) = \delta \dot{\gamma}(t)$ and $\beta_n(t) = k_n \alpha_n(t)$. The equation of motion for $\delta \dot{\gamma}(y,t) = \partial \delta u(y,t) / \partial y$ is the same as for $\delta u(y,t)$. This follows simply by differentiation of both sides of Eq. (13) with respect to y ,

$$\rho \frac{\partial \delta \dot{\gamma}(y,t)}{\partial t} = \frac{d\sigma(\dot{\gamma}_0)}{d\dot{\gamma}_0} \frac{\partial^2 \delta \dot{\gamma}(y,t)}{\partial y^2} - \kappa(\dot{\gamma}_0) \frac{\partial^4 \delta \dot{\gamma}(y,t)}{\partial y^4}. \quad (21)$$

Substitution of the cosine-series expansion (20) yields

$$\frac{d\beta_n(t)}{dt} = - \left[\frac{d\sigma(\dot{\gamma}_0)}{d\dot{\gamma}_0} + \kappa(\dot{\gamma}_0) k_n^2 \right] \frac{k_n^2}{\rho} \beta_n(t). \quad (22)$$

The linearized constraint (9) under controlled stress conditions in terms of the cosine-Fourier coefficients $\beta_n(t)$ is found from Eqs. (4) and (20),

$$\sum_{n=0}^{\infty} (-1)^n \beta_n(t) \left[\frac{d\sigma(\dot{\gamma}_0)}{d\dot{\gamma}_0} + \kappa(\dot{\gamma}_0) k_n^2 \right] = 0. \quad (23)$$

It is shown in the Appendix that the equation of motion that incorporates the constraint is given by

$$\frac{d\beta_n(t)}{dt} = \sum_{m=0}^{\infty} C_m \frac{k_m^2}{\rho} \left[\delta_{nm} - \frac{(-1)^{n+m} C_n C_m}{\sum_{j=0}^{\infty} C_j^2} \right] \beta_m(t), \quad (24)$$

with δ_{ij} the Kronecker delta and

$$C_n \equiv - \left[\frac{d\sigma(\dot{\gamma}_0)}{d\dot{\gamma}_0} + \kappa(\dot{\gamma}_0) k_n^2 \right]. \quad (25)$$

The last term between the square brackets in Eq. (24) describes the coupling between coefficients due to the imposed constraint. Multiplying both sides of Eq. (24) with $\beta_n(t)$ and summing over n yields

$$\frac{1}{2} \frac{d}{dt} \sum_{n=0}^{\infty} \beta_n^2(t) = \sum_{m=0}^{\infty} C_m \frac{k_m^2}{\rho} \left[\beta_m^2(t) - \frac{\sum_{n=0}^{\infty} (-1)^n \beta_n C_n}{\sum_{j=0}^{\infty} C_j^2} (-1)^m \beta_m C_m \right]. \quad (26)$$

The system is unstable if and only if $(d/dt) \sum_{n=0}^{\infty} \beta_n^2(t) > 0$. A constraint stabilizes a system, since it diminishes the space of admissible solutions for the equation of motion, or it has no stabilizing effect when the unstable solutions of the unconstrained equation of motion are also unstable under the constrained motion. The unconstrained equation of motion is unstable if and only if $C_1 > 0$, as was shown in Sec. IV A. Hence, if we can show that the constrained equation of motion is unstable when $C_1 > 0$, it follows that the constraint has no stabilizing effect, and the stability criterion is exactly the same as for the unconstrained system. When $C_1 > 0$ the following choice for the coefficients is unstable: $\beta_1 \neq 0$, $\beta_n = 0$ for $n > 1$, while β_0 should be chosen to satisfy the constraint (23). To see that this choice is an unstable one, we find from Eq. (26) (note that $k_0 = 0$)

$$\frac{1}{2} \frac{d}{dt} \sum_{n=0}^{\infty} \beta_n^2(t) = C_1 \frac{k_1^2}{\rho} \beta_1^2 \left[1 - \frac{C_1^2}{\sum_{j=0}^{\infty} C_j^2} \right]. \quad (27)$$

The term between the square brackets is positive, so that the time derivative is indeed positive when $C_1 > 0$. The stability criterion for controlled stress experiments is therefore the same as for controlled shear experiments.

V. LACK OF UNIQUE SHEAR-BANDED STRUCTURE FOR THE TWO-PLATE GEOMETRY

The Navier-Stokes equation (7) is a fourth-order differential equation in $u(y,t)$ [third order in $\dot{\gamma}(y,t)$] with only two boundary conditions (8) or (9), and $u(y=0,t) = 0$. This implies that many stable stationary states exist (or no stationary state exists at all), and the stationary shear-banded structure is therefore not uniquely determined. The stationary state that is selected is determined by the initial conditions to the equation of motion (7). A specific stationary shear-banded structure depends on the initial conditions, and can only be found by time integration of the full nonlinear equation of motion (7), subject to the boundary condition (8) or (9), which specifies either controlled shear or controlled stress conditions. The final shear-banded state thus depends on the particular initial state of the system.

Intuitively this degeneracy can be understood as follows. When a particular interface between two bands satisfies the Navier-Stokes equation, one is free to connect bands by such an interface in any way possible, provided the constraints are satisfied. A shear-banded structure may be constructed by

connecting these “building blocks” (interface and bands of constant shear rate) in the many possible ways that satisfy the constraints.

The degeneracy may be a special feature of the two-plate geometry. In a Couette geometry there are additional terms in the equation of motion, which may drive interfaces in a particular direction. This would ultimately lead to a unique shear-banded structure with a single interface. The two-plate geometry is an idealized mathematical conception. It may well be that additional terms in the Navier-Stokes equation in the case of real geometries may drive the system towards a unique stationary state. This will be a subject for further study.

When the initial state includes Fourier components close to the most rapidly growing mode with wave number k_{max} , the flow will have a generic structure after some time, where the number of bands is of the order l/λ_{max} , with $\lambda_{max} = 2\pi/k_{max}$. The most rapidly growing Fourier mode will dominate the structure after some time, and thus selects the particular shear-banded structure that will exist at later times. The degeneracy of the stationary state is now the result of different positions of the bands in the initial stage. There are thus many different initial conditions that will give rise to similar stationary shear-banded structure. The nonuniqueness of the final shear-banded structure implies that stationary states are not stable in the sense that each perturbation changes the details of a stationary state.

The above discussion will be made more explicit in the following section, where the equation of motion is integrated numerically. Notice that integration of the full equation of motion is the only way to predict the final state of the system.

VI. NUMERICAL INTEGRATION OF THE EQUATION OF MOTION

The velocity can be expanded in a sine series on the interval $[-l, l]$ as

$$u(y, t) = \dot{\gamma}(t)y + \sum_{n=0}^{\infty} \alpha_n(t) \sin\{k_n y\}, \quad (28)$$

where the wave numbers are given in Eq. (15). This general form incorporates the boundary condition $u(y=0, t) = 0$ at the lower plate. The additional conditions (8), (9) imply

$$\dot{\gamma}(t) = \dot{\gamma}_0, \quad (29)$$

$$\begin{aligned} & \sigma \left(\dot{\gamma}(t) + \sum_{n=1}^{\infty} (-1)^n \alpha_n(t) k_n \right) \\ & + \kappa \left(\dot{\gamma}(t) + \sum_{n=1}^{\infty} (-1)^n \alpha_n(t) k_n \right) \sum_{n=1}^{\infty} (-1)^n \alpha_n(t) k_n^3 \\ & = \sigma_0 = \sigma(\dot{\gamma}_0). \end{aligned} \quad (30)$$

The first condition applies under controlled shear conditions; the second under controlled stress conditions.

Under controlled shear conditions the constraint (29) is trivially accounted for by simply replacing the overall shear rate $\dot{\gamma}(t)$ in Eq. (28) by the constant $\dot{\gamma}_0$. Under controlled

stress conditions it is more convenient to solve the Navier-Stokes equation for the local shear rate, which is found from Eq. (7) by differentiation of both sides with respect to y . From the sine Fourier representation (28) for the velocity, it follows that the shear rate is of the form

$$\dot{\gamma}(y, t) = \sum_{n=0}^{\infty} \beta_n(t) \cos\{k_n y\}, \quad (31)$$

with $\beta_0(t)$ equal to the overall shear rate $\dot{\gamma}(t)$. In solving the Navier-Stokes equation (7), one must insist on the constraint (30), which now reduces to

$$\begin{aligned} & \sigma \left(\sum_{n=0}^{\infty} (-1)^n \beta_n(t) \right) - \sigma_0 \\ & + \kappa \left(\sum_{n=0}^{\infty} (-1)^n \beta_n(t) \right) \sum_{n=1}^{\infty} (-1)^n \beta_n(t) k_n^2 = 0. \end{aligned} \quad (32)$$

It is shown in the Appendix how to implement this constraint in a numerical solution of the Navier-Stokes equation.

We shall have to specify σ as a function of $\dot{\gamma}$. The most satisfying approach would be to derive the shear rate dependence of the shear viscosity from microscopic considerations, as is done in Refs. [25,26] for entangled polymer systems. Here we shall construct a simple constitutive equation for σ , which mimics experimental results. The generic form exhibits a van der Waals-like behavior. Since the shear viscosity η is an even function of the shear rate, probably the most simple form reads

$$\eta(\dot{\gamma}) = \frac{\eta_0 + \alpha \eta_{\infty} \dot{\gamma}^2}{1 + \alpha \dot{\gamma}^2}, \quad (33)$$

where the zero- and high shear rate limiting viscosities η_0 and η_{∞} are introduced, and where α is a parameter that can be chosen such that typical experimental data are reproduced. Here we use $\eta_0 = 20$ Pa s, $\eta_{\infty} = 1$ Pa s, and $\alpha = \frac{1}{20} \text{ s}^2$. This choice leads to a functional form of the shear stress σ versus shear rate that is quite similar to experimental results for wormlike micelles [6], and is plotted in Fig. 3(a). The horizontal line corresponds to the modified Maxwell equal area construction (10).

We also have to specify the shear-curvature viscosity κ as a function of $\dot{\gamma}$. Like the shear viscosity, κ is an even function of the shear rate. There are so far no experimental or theoretical values known for κ . Here, we will assume that no shear banding occurs when the gap width is reduced by a factor of 10, implying that $2\pi/k_{crit} = \lambda_{crit} = l/10$. For a given overall shear rate $\dot{\gamma}_0$, Eq. (17) then specifies the value of $\kappa(\dot{\gamma} = \dot{\gamma}_0)$. We need not specify the gap width in the numerical solution of the equation of motion when y is expressed in units of l . The typical number of shear bands in the initial stage is now found to be equal to $l/\lambda_{max} = 7$. As discussed in Sec. II, the shear-curvature viscosity κ tends to zero for shear rates where the shear viscosity tends to its high shear limit. Since κ is an even function of the shear rate, and

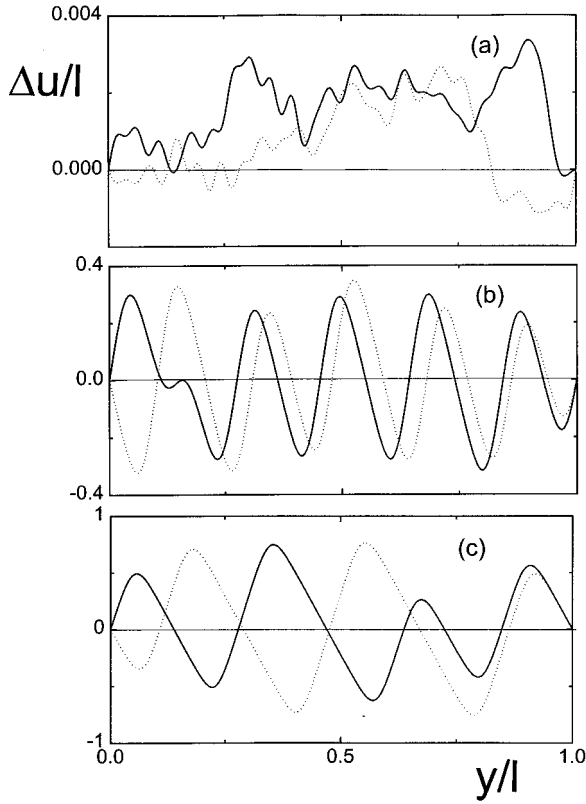


FIG. 4. The flow velocity $\Delta u(y,t) \equiv u(y,t) - \dot{\gamma}_0 y$ divided by the gap width l in units of seconds as a function of y/l for various times in case of controlled shear conditions: (a) $\tau=0$, (b) $\tau=0.4$, and (c) the stationary state. The initial profiles in (a) are randomly generated.

shear thins to zero in the same shear rate range as the shear viscosity, the simplest form for κ is $\kappa \sim \eta(\dot{\gamma}) - \eta_0$, and hence,

$$\kappa(\dot{\gamma}) = \frac{\kappa_0}{1 + \alpha \dot{\gamma}^2}, \quad (34)$$

where $\kappa_0 = \kappa(\dot{\gamma} \rightarrow 0)$. In the case $\dot{\gamma}_0 = 10 \text{ s}^{-1}$, we have stability on decreasing the gap width by a factor of 10 for $\kappa_0/l^2 = 1.688 \times 10^{-3} \text{ N s}$. A plot of the shear-curvature viscosity κ is given in Fig. 3(b).

Note that the numerical value of $\kappa(\dot{\gamma}_0)\pi^2/l^2$ is usually small in comparison to $|d(\dot{\gamma}_0)/d\dot{\gamma}_0|$, so that the instability criterion $d\sigma(\dot{\gamma}_0)/d\dot{\gamma}_0 < -\kappa(\dot{\gamma}_0)\pi^2/l^2$ virtually amounts to $d\sigma(\dot{\gamma}_0)/d\dot{\gamma}_0 < 0$. The stability limiting shear rates are therefore almost equal to the shear rates where σ in Fig. 3(a) exhibits extremum values.

The number of Fourier modes used in all calculations is 50. Adding more Fourier components does not change flow velocities or shear rates to within a percent. The dimensionless time $\tau = t\eta_0/\rho l^2$ will be used in the sequel, which is the time in units of the typical relaxation time towards a homogeneously sheared state in the case where the system would have been stable.

A. Controlled shear conditions

Numerical results for the difference $\Delta u(y,t) \equiv u(y,t) - \dot{\gamma}_0 y$ are given in Fig. 4 as a function of y for different

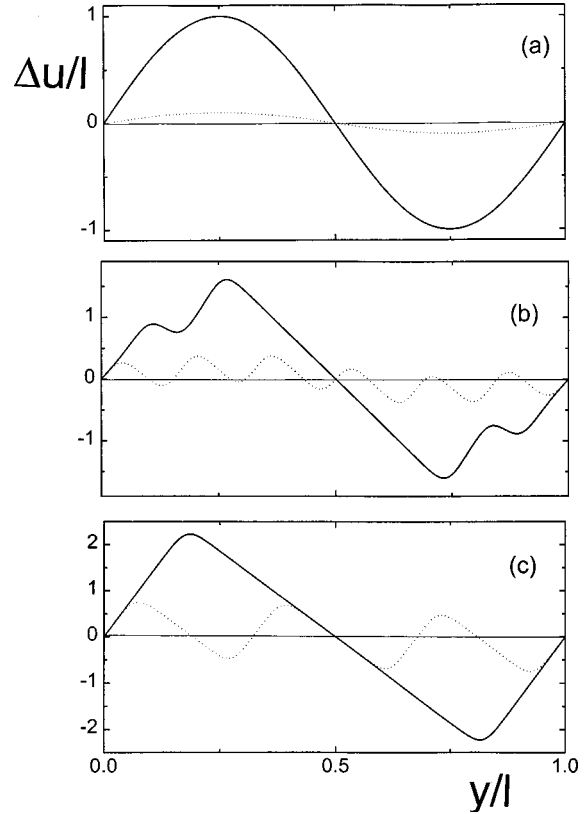


FIG. 5. Same as in Fig. 4. The solid line in (a) is an initial state with a large amplitude; the dotted line is an initial state with the same wavelength but a much smaller amplitude. In (b) the states are shown for $\tau=0.4$. The stationary states are given in (c).

times. The overall shear rate is equal to $\dot{\gamma}_0 = 10 \text{ s}^{-1}$. The temporal evolution of two randomly generated initial states is depicted. The initial states are given in Fig. 4(a). In generating these initial states, the Fourier coefficients α_n are randomly chosen in the interval $\pm 0.01/n$, where division by n ensures an equal average contribution of each Fourier mode to the stress $\sigma(t=0)$. The two initial states are seen to be quite different. In Fig. 4(b) the state for $\tau=0.4$ is depicted. As can be seen, the most rapidly growing Fourier mode dominates the state of the system at this time. The stationary states are depicted in Fig. 4(c) (the stationary state is typically attained for $\tau \approx 6-8$). Coexistence between bands with a constant shear rate is found. The shear rates $\dot{\gamma}_{\pm}$ in the high and low shear rate regions and the constant stress Σ_{stat} are in accordance with the modified Maxwell equal area construction (10). The number of bands in the stationary states are approximately the same due to dominance of the most rapidly growing Fourier mode in the initial stages of demixing, as depicted in Fig. 4(b). Note that the number of bands in the stationary state is less than the number of bands in the initial stage. The nonlinear terms in the Navier-Stokes equation thus tend to reduce the number of bands that are initially formed. Typically one finds 6 to 7 interfaces.

The number of bands in the initial stage is determined by the most rapidly growing Fourier mode only when this mode has the opportunity to become dominant. When another wavelength is dominant right from the start, the number of bands in the stationary state is determined by the wavelength of that mode. This is depicted in Fig. 5. The solid line in Fig.

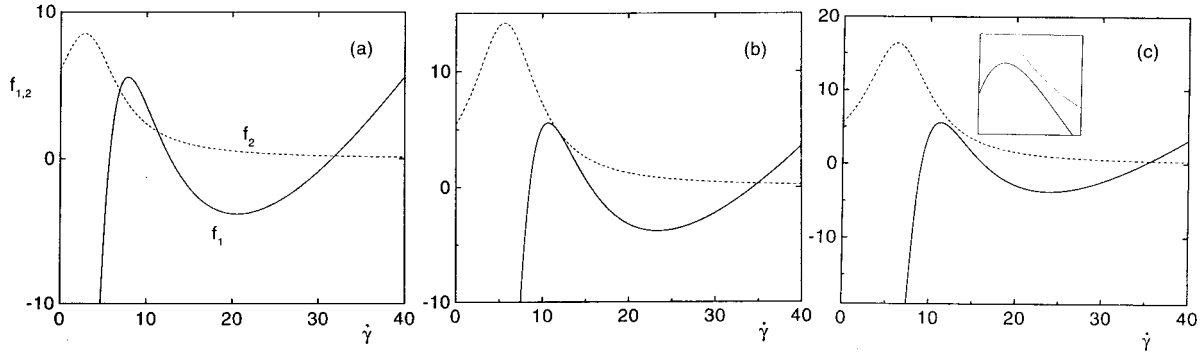


FIG. 6. The solid line is the function f_1 in Eq. (36), while the dotted line is the function f_2 in Eq. (37). The points of intersection give the overall shear rates for which the constraint (32) is satisfied. There are generally three intersection points due to the van der Waals-like behavior of f_1 , as depicted in (a). When f_1 and f_2 are tangential in a point, see (b), there are only two intersection points. This happens when two constraint branches cross. In (c) there is only a single overall shear rate that satisfies the constraint.

5(a) is an example of a large initial perturbation that remains dominant for all times. In the initial stage in Fig. 5(b), where $\tau=0.4$, the most rapidly growing Fourier mode does turn up, but does not become dominant. In the stationary state in Fig. 5(c) there are only two interfaces, in accordance with the symmetry of the initial state. A perturbation with the same wavelength but with a much smaller amplitude [the dotted line in Fig. 5(a)] evolves quite differently in time. Now the most rapidly growing Fourier mode dominates the structure in the initial stage, as depicted in Fig. 5(b), and the final stationary state in Fig. 5(c) exhibits the typical 6 to 7 interfaces as in Fig. 4(c). These results comply with the remarks in Sec. V on the degeneracy of the stationary state in the two-plate geometry.

It is also found that the shear-banding transition can occur outside the range of unstable shear rates, provided that the amplitude of the initial perturbation is large enough. One can therefore probably distinguish between spinodal shear rates (which are the linear stability limiting shear rates) and binodal shear rates (which are the shear rates beyond which the transition cannot occur).

B. Controlled stress conditions

The constraint (32) is most conveniently written as

$$f_1(\dot{\gamma}) = f_2(\dot{\gamma}), \quad (35)$$

with

$$f_1(\dot{\gamma}) = \sigma \left(\dot{\gamma} + \sum_{n=1}^{\infty} (-1)^n \beta_n \right) - \sigma_0, \quad (36)$$

$$f_2(\dot{\gamma}) = -\kappa \left(\dot{\gamma}(t) + \sum_{n=1}^{\infty} (-1)^n \beta_n(t) \right) \sum_{n=1}^{\infty} (-1)^n \beta_n(t) k_n^2. \quad (37)$$

For a given set of β_n 's with $n > 0$, the intersection points of f_1 and f_2 as functions of $\dot{\gamma} = \beta_0$ thus give the overall shear rates for which the constraint is satisfied. A typical plot of these functions is given in Fig. 6. Due to the van der Waals-like behavior of σ there are generally three overall shear rates that satisfy the constraint [see Fig. 6(a)], although it

may happen that there are only two solutions [see Fig. 6(b)] or even a single solution [see Fig. 6(c)]. A typical temporal evolution of these three constraint branches is given in Fig. 7, where the thick solid line is the actual overall shear rate, and the thin solid lines are the remaining shear rates that satisfy the constraint. When two branches cross, the two functions f_1 and f_2 are tangential at an intersection point, as depicted in Fig. 6(b). The surprising thing now is that no convergence to a stationary state is found. The actual shear rate always remains on a branch that does not lead to a proper stationary state where the stress is constant throughout the gap, equal to the imposed stress at the upper plate. Instead, what we find is that after some time the stress becomes equal to the modified Maxwell equal area stress throughout the gap, except very close to the upper plate, where the stress very rapidly adjusts to match the imposed stress. The most rapidly varying Fourier mode that is used determines the width of the region near the upper plate where the stress changes from the modified Maxwell equal area stress to the imposed stress. The conclusion is therefore that there is no convergence to a proper stationary state under controlled stress conditions. One way out of this dilemma could be to introduce a fluctuating term to the stress. This is physically plausible, since the shear-curvature contribution

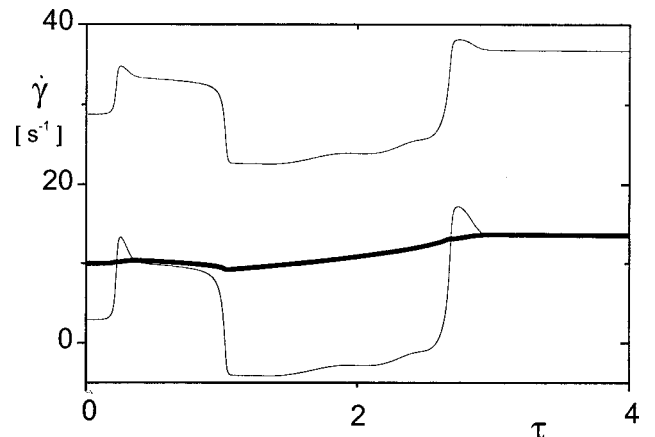


FIG. 7. The temporal evolution of the actual overall shear rate (thick solid line) and the other overall shear rates that satisfy the constraint (32) (thin lines).

to the stress is the result of the variation of shear rates over microstructural length scales. These fluctuations may cause the shear rate to change to another branch when two branches cross. Without fluctuations, switching to another branch is impossible due to the continuous differentiability of $\dot{\gamma}(t)$ as a function of time. For example, changing to another branch at $\tau \approx 0.35$ in Fig. 7 implies a jump discontinuity of $d\dot{\gamma}(t)/dt$. When adding fluctuations to the equation of motion, however, again nonconvergence is found, with the same features as before without fluctuations. The inevitable conclusion is that the simple one-dimensional equation of motion is insufficient to describe shear banding under controlled stress conditions. Flow inhomogeneities in the two other dimensions (along the flow and vorticity directions) must be incorporated. The only paths that lead to a proper stationary state are those with flow gradients in the flow and/or vorticity direction. The full three-dimensional Navier-Stokes equation should be investigated for shear banding under controlled stress conditions. The simplest generalization of the constitutive relation (4) to three dimensions that one can use in such an investigation is probably

$$\begin{aligned} \Sigma(\mathbf{r}, t) = & [\eta(\dot{\gamma}(\mathbf{r}, t)) - \kappa(\dot{\gamma}(\mathbf{r}, t))\nabla^2] \\ & \times [(\nabla\mathbf{u}(\mathbf{r}, t)) + (\nabla\mathbf{u}(\mathbf{r}, t))^T], \end{aligned} \quad (38)$$

where the superscript T stands for ‘‘the transpose of.’’ The analysis of the full three-dimensional Navier-Stokes equation is a subject for future work.

VII. SUMMARY AND DISCUSSION

In order to describe shear banding, an additional term to the total stress is introduced. This term relates to shear induced spatial variations in the microstructure on length scales of the order of the microstructural correlation length. The corresponding proportionality constant is referred to here as *the shear-curvature viscosity*, which is shown to shear thin to zero at the same shear rate where the shear viscosity attains its high shear limiting value. Under controlled shear conditions the extended constitutive relation leads to a modified Maxwell equal area construction that gives the shear rates in the low and high shear bands together with the stress as attained in the stationary state. The constitutive relation that includes the shear-curvature induced stress gives rise to shear banding in the two-plate geometry under controlled shear conditions. In the initial stage of the shear-banding transition there is a most rapidly growing Fourier mode that determines the number of shear bands in the stationary state. Both the number of bands and the width of the bands are determined by the shear-curvature viscosity and shear viscosity characteristics. The stationary state in the two-plate geometry is not uniquely determined, but depends on the initial unstable perturbation. When the amplitude of the initial perturbation is very large, the number of bands is dictated by the characteristic wavelength of the initial state. The shear-banding transition can also occur outside the region of unstable shear rates, when the amplitude of the initial perturbation is large enough. Under controlled stress conditions no stable stationary state could be found, even when fluctuating terms were added to the Navier-Stokes equation. Probably flow variations in the flow- and vorticity directions

are essential under controlled stress conditions.

The above findings raise a few questions that should be considered in future work:

(a) There are additional terms in the Navier-Stokes equation for a Couette geometry. These terms could lead to a preferred drift velocity of interfaces and thereby ultimately lead to a single, unique shear-banded state with just a single interface.

(b) What is the mechanism that makes flow variations along the flow- and vorticity directions in the two-plate geometry essential to reach a stationary state? A feature of the one-dimensional flow considered here is that $\mathbf{u} \cdot \nabla\mathbf{u} = 0$. Since $\nabla\mathbf{u}$ is large within the interfaces, a small contribution of \mathbf{u} along the flow- or vorticity directions can lead to appreciable contributions to the three-dimensional Navier-Stokes equation. It might be that the additional terms to the Navier-Stokes equation in a Couette geometry make such flow variations redundant for obtaining a proper stationary state. In any case it seems worthwhile to study the three-dimensional Navier-Stokes equation, since this is the equation that should be used to study (thermodynamically driven) phase transitions under shear flow.

(c) Where are the binodal shear rates located and how do the minimum amplitude and the optimum wavelength of the initial perturbation, leading to demixing outside the unstable region, vary with the shear rate?

(d) What are the actual numerical values of the shear-curvature viscosity of real systems, and how can it be measured? One might be able to probe the wavelength of the most rapidly growing Fourier mode or its growth rate, or to measure the interfacial width in the stationary state. In order to obtain the shear-curvature viscosity from such data, one also needs to measure the entire van der Waals loop of σ versus $\dot{\gamma}$ in a geometry with a gap width that is smaller than the smallest unstable wavelength. It will depend on actual values of the shear-curvature viscosity whether this is feasible.

(e) So far there have been no theoretical predictions for the shear-curvature viscosity. Since this coefficient relates to very rapid spatial microstructural changes, such calculations will probably be more complex than shear viscosity calculations.

ACKNOWLEDGMENTS

Recently ideas similar to those discussed in the present paper were formulated in a preprint database [20]. Dr. Paul van der Schoot is acknowledged for pointing me to that database. This work has benefited from discussions with Professor Wim Briels.

APPENDIX

In this appendix it is shown how to construct the solution of equations of motion under a constraint. Consider an equation of motion of the form

$$\frac{d\mathbf{x}}{dt} = \mathbf{f}(\mathbf{x}), \quad (A1)$$

where \mathbf{x} is an N -dimensional vector. For our purpose, \mathbf{x} is the vector $(\beta_0, \beta_1, \dots)$ of the Fourier amplitudes in Eq. (31)

for the shear rate $\dot{\gamma}(y,t)$. The field \mathbf{f} is a (linear or nonlinear) vector field of \mathbf{x} , whose explicit form follows from the cosine Fourier expansion of the right-hand side of the Navier-Stokes equation (7) in the range $y \in [-l, +l]$, after first having differentiated with respect to y . Let

$$\Phi(\mathbf{x}) = 0 \quad (\text{A2})$$

be a scalar constraint to the equation of motion (A1). For our purpose the scalar field Φ is the function given in Eq. (32). The vector $d\mathbf{x}/dt$ is tangential to the hypersurface spanned by the constraint (A2). Since $\nabla\Phi$ is perpendicular to that hypersurface, we have that $\nabla\Phi(\mathbf{x}) \cdot d\mathbf{x}/dt = 0$. Let $\hat{\mathbf{I}}$ denote the unit tensor. Multiplying both sides of Eq. (A1) with the projection operator,

$$\mathbf{P} \equiv \hat{\mathbf{I}} - \frac{[\nabla\Phi(\mathbf{x})][\nabla\Phi(\mathbf{x})]}{|\nabla\Phi(\mathbf{x})|^2}. \quad (\text{A3})$$

this operator projects a vector onto the hypersurface and thus leaves the left-hand side of the equation of motion (A1) unchanged, so that

$$\frac{d\mathbf{x}}{dt} = \left[\hat{\mathbf{I}} - \frac{[\nabla\Phi(\mathbf{x})][\nabla\Phi(\mathbf{x})]}{|\nabla\Phi(\mathbf{x})|^2} \right] \cdot \mathbf{f}(\mathbf{x}). \quad (\text{A4})$$

This is the equation of motion that can be solved without any further constraint, and ensures that the constraint (A2) is satisfied.

In the linear stability analysis in Sec. IV B, the equation of motion (22) reads

$$\frac{d\beta_n(t)}{dt} = C_n \frac{k_n^2}{\rho}, \quad (\text{A5})$$

with C_n given by Eq. (25). Furthermore, the vector $\nabla\Phi$ follows directly from Eq. (23) as

$$\nabla_n \Phi = (-1)^{n+1} C_n. \quad (\text{A6})$$

Substitution of these forms into Eq. (A4) yields the equation of motion (24).

-
- [1] S. Hess, Z. Naturforsch. A **30**, 728 (1975); **30**, 1224 (1975); **31**, 1507 (1976).
- [2] P.D. Olmsted and P.M. Goldbart, Phys. Rev. A **41**, 4578 (1990); **46**, 4966 (1992).
- [3] P.D. Olmsted and C.-Y.D. Lu, Phys. Rev. E **56**, 55 (1997).
- [4] V. Schmitt, F. Lequeux, A. Pousse, and D. Roux, Langmuir **10**, 955 (1994).
- [5] J.-F. Berret, D.C. Roux, and G. Porte, J. Phys. II **4**, 1261 (1994).
- [6] P.T. Callaghan, M.E. Cates, C.J. Rofe, and J.B.A.F. Smulders, J. Phys. II **6**, 375 (1996).
- [7] P. Boltenhagen, Y. Hu, E.F. Matthys, and D.J. Pine, Phys. Rev. Lett. **12**, 2359 (1997).
- [8] O. Diat, D. Roux, and F. Nallet, J. Phys. II **3**, 1427 (1993); D. Roux, F. Nallet, and O. Diat, Europhys. Lett. **24**, 53 (1993).
- [9] D. Bonn, J. Meunier, O. Greffier, A. Al-Kahwaji, and H. Kellay, Phys. Rev. E **58**, 2115 (1998).
- [10] A. Imhof, A. van Blaaderen, and J.K.G. Dhont, Langmuir **10**, 3477 (1994).
- [11] S. von Hüberbein, M. Würth, and T. Palberg, Prog. Colloid Polym. Sci. **100**, 241 (1996).
- [12] T. Palberg and M. Würth, J. Phys. I **6**, 237 (1996).
- [13] T.C.B. McLeish and R.C. Ball, J. Polym. Sci., Part B: Polym. Phys. **24**, 1735 (1986).
- [14] T.C.B. McLeish, J. Polym. Sci., Part B: Polym. Phys. **25**, 2253 (1987).
- [15] M. Doi and S.F. Edwards, J. Chem. Soc., Faraday Trans. 2 **74**, 1802 (1978); **74**, 1818 (1978); **75**, 38 (1979).
- [16] M. Doi, J. Polym. Sci., Polym. Phys. Ed. **19**, 229 (1981).
- [17] H. Kuzuu, M. Doi, J. Phys. Soc. Jpn. **52**, 3486 (1983).
- [18] N.A. Spenley, X.F. Yuan, and M.E. Cates, J. Phys. II **6**, 551 (1996).
- [19] G. Porte, J. Berret, and J. Harden, J. Phys. II **7**, 459 (1997).
- [20] P.D. Olmsted and C.-Y.D. Lu, preprint cond-mat/9901226.
- [21] P. Nozieres and D. Quemada, Europhys. Lett. **2**, 129 (1986).
- [22] V. Schmitt, C.M. Marques, and F. Lequeux, Phys. Rev. E **52**, 4009 (1995).
- [23] J.W. Cahn and J.E. Hilliard, J. Chem. Phys. **28**, 258 (1958); **31**, 688 (1959).
- [24] J.K.G. Dhont, J. Chem. Phys. **105**, 5112 (1996). This paper discusses a microscopic derivation of the Cahn-Hilliard equation for colloidal systems.
- [25] N.A. Spenley, M.E. Cates, and T.C.B. McLeish, Phys. Rev. Lett. **71**, 939 (1993).
- [26] M.E. Cates, T.C.B. McLeish, and G. Marrucci, Europhys. Lett. **21**, 451 (1993).